Weather-Induced Transport through a Tidal Channel Calibrated by an Unmanned Boat

CHUNYAN LI, EDDIE WEEKS, WEI HUANG, AND BRIAN MILAN

Department of Oceanography and Coastal Sciences, Coastal Studies Institute, Louisiana State University, Baton Rouge, Louisiana

RENHAO WU

College of Marine Science and Technology, Zhejiang Ocean University, Zhejiang, China

(Manuscript received 31 July 2017, in final form 20 November 2017)

ABSTRACT

An unmanned surface vehicle (USV) was designed and constructed to operate continuously for covering both flood and ebb and preferably a complete tidal cycle (e.g., ~24 h) to measure the vertical profiles of horizontal flow velocity. It was applied in a tidal channel at Port Fourchon, Louisiana. A bottom-mounted ADCP was deployed for 515 days. The first EOF mode of the velocity profiles showed a barotropic type of flow that explained more than 98.2% of the variability. The second mode showed a typical estuarine flow with two layers, which explained 0.47% of the variability. Using a linear regression of the total transport from the USV with the vertically averaged velocity from the bottom-mounted ADCP, with an R-squared value of 98%, the total along-channel transport throughout the deployment was calculated. A low-pass filtering of the transport allowed for examining the impact of 76 events with cold, warm, or combined cold–warm fronts passing the area. The top seven most severe events were discussed, as their associated transports obviously stood out in the time series, indicating the importance of weather. It is shown that large-scale weather systems with frontal lines of ~1500–3000-km horizontal length scale control the subtidal transport in the area. Cold (warm) fronts tend to generate outward (inward) transports, followed by a rebound. The maximum coherence between the atmospheric forcing and the ocean response reached ~71%–84%, which occurred at about a frequency f of ~0.29 cycle per day or T of ~3.4 days in the period, consistent with the atmospheric frontal return periods (~3–7 days).

1. Introduction

Measurements of flow velocity are required for estimations of flushing time; fluxes of water, salt, suspended sediments; and other waterborne materials, either dissolved or suspended. A bottom-mounted acoustic Doppler current profiler (ADCP) or current meter within a tidal channel can record flow velocity continuously over a long period of time. An ADCP mounted on a vessel can also provide information about the flow and integrated total transport (e.g., Zhu et al. 2001; Andrade et al. 2003; Osiński et al. 2003; Waterhouse and Valle-Levinson 2010; Firing et al. 2011; Chaigneau et al. 2013; Barton et al. 2015; Zhu et al. 2017). In coastal waters, the latter approach is usually implemented by running the vessel along a transect line repeatedly over at least a complete tidal cycle (e.g., Valle-Levinson et al. 1998, 2007; Li 2002, 2006, 2013; Kang and Di Iorio 2008; Li et al. 2011b; Li and Chen 2014). The pros and cons of these two methods are readily seen: in the first method, the instrument is fixed at one location and can provide a long time series of flow data. It, however, cannot resolve the spatial structure of the flow and cannot obtain an accurate quantification of the total transport. In the second method, the instrument moves with the vessel and thus can provide detailed flow structure and an accurate estimate of the total transport along the transect if sufficient repetitions are made within a complete tidal cycle and possible aliasing is reduced to a minimum. Such observations are, however, usually more expensive, labor intensive, and weather dependent, and thus not feasible for long-term observations except under some special circumstances, such as when a commercial ship (e.g., a ferry) is used as a moving platform of observations

Corresponding author: Renhao Wu, mikewu@zjou.edu.cn

DOI: 10.1175/JTECH-D-17-0130.1

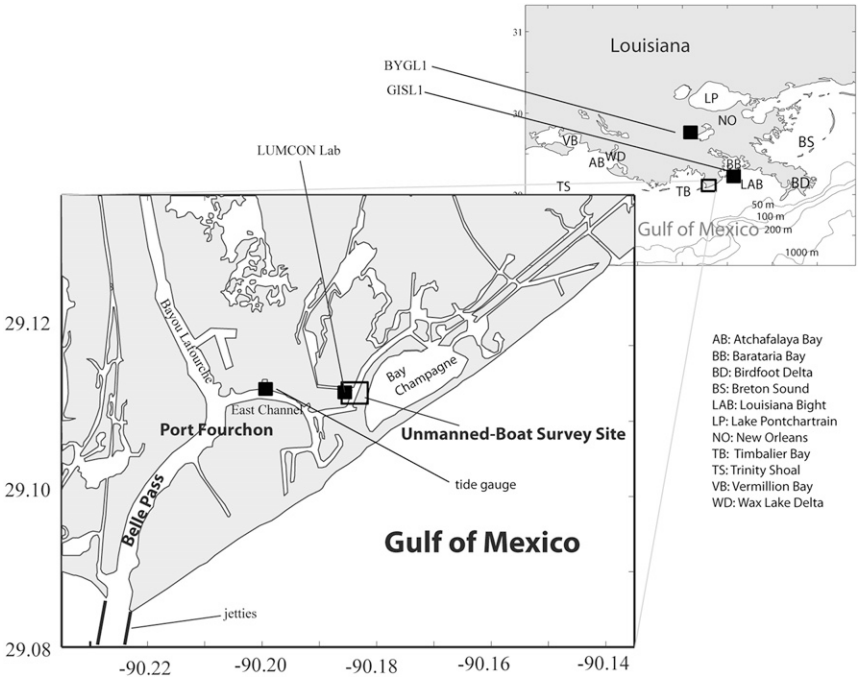

FIG. 1. Study site. Unmanned-boat (USV) survey area is shown in the rectangular, where a bottom-mounted ADCP was deployed from October 2006 to April 2008.

(Buijsman and Ridderinkhof 2007a,b; Codiga and Aurin 2007). In most waterways, such vessel-based observations are usually done by researchers using a small research vessel limited in a relatively short period (e.g., Li 2002, 2006). Another limitation of a vessel-based survey is that it can be a challenge to ensure accurate coverage of the same transect line each time, as the current can be swift during peak flood and ebb and the boat operator can experience fatigue during a long period of repetition along a planned route. This can lead to inaccuracy in repeating the transect line and introduce additional errors in flow structure.

To provide an accurate and long-term estimate of the total transport, we may combine the two approaches: a mooring ADCP records a long time series of flow data, while an ADCP mounted on a vessel runs across a transect passing the location where the instrument is deployed and records the spatial structure of flow profiles and thus the total transport; the transport is then correlated with the flow data from the moored ADCP. By doing this, regression coefficients can be obtained so that we can calculate the total transport for the entire dataset from the mooring data.

This study implements such a method with an unmanned platform for cross-channel observations: we use an unmanned surface vehicle (USV) for accurate measurements of the cross-channel structure of the along-channel flows. The goal is to obtain a time series of the transport of water through a tidal channel at Port Fourchon, Louisiana, to determine the impact of weather on the total transport. The use of an automated USV with a high-resolution GPS allowed for a very accurate repetition of a planned survey route with 10 cross sections over an entire tidal cycle across a tidal channel for more than 1500 times, which would not be possible with a manned vessel, of which a few hundred crossings near a bottom-mounted ADCP were used in the analysis. We will first introduce the study area and the observational tool before the discussion of its application and results.

2. Study area

The study was conducted from 2006 through 2008. The study area (Fig. 1) is at the southern Louisiana coast, about 6 km from the coastal ocean through some narrow tidal waterway. The waterway goes through 1) the East Channel, a channel bifurcated from the ~230–300-m-wide Bayou Lafourche; 2) Belle Pass; and 3) the ~800-m-long jetties, before connecting with the coastal ocean. The survey area is by the Fourchon Laboratory of the Louisiana Universities Marine Consortium (LUMCON). It is in a tidal channel with a depth between 2 and 15 m. The width of the channel was about ~60–80 m at the time of the survey. The channel is connected in its east-northeast region to Bay Champagne (Fig. 1) and a few bayous. There is a ~100-m-wide low-level

salt marsh zone separating much of the channel from Bay Champagne, except where the vegetation disappears in the north, at which point the channel and Bay Champagne are narrowly connected. Bay Champagne is a semicircular and semienclosed shallow water of mostly less than 1.5-m depth not directly connected to the coastal ocean. It has a dimension of ~1.5 km × 0.6 km. There is no major river or freshwater source. This area is characterized by diurnal microtides (Kantha 2005) with a maximum tidal range of ~0.6 m and thus the wind influence to the water transport is expected to be relatively significant. Since the adjacent estuaries and bayous are crucial to fish nursery, there has been a great deal of interest in wind-induced water and thus larvae transport (e.g., Norcross and Shaw 1984; Kupchik 2014).

3. Method

In this study a USV was used for the measurements of the cross-sectional flow structure and for an accurate measurement of transport. The existing technology allows only the USV to do the data collection for a few days (Weeks et al. 2011) versus a few months—a period typical for bottom-deployed ADCPs. It was proposed in this study that we combine the two—the bottom-mounted ADCP (deployed for a few months) and the ADCP mounted on the USV (used for at least a few hours but preferably covering an entire tidal cycle or longer). Thus, we can calibrate the flowmeter as a "transport sensor." Obviously, this method has an underlying assumption, that is, the relation between the USV-measured transport and the flow velocity from the bottom-mounted ADCP can be linked by a regression and the regression coefficients do not change with time when the transport changes over time. For the simplest case, the mean velocity from the bottom-mounted ADCP is linearly proportional to the integrated transport measured from the ADCP on the USV. Therefore, the main idea of this study is to use the USV to calibrate a bottom-mounted ADCP as a transport sensor by a short-term survey, so we can obtain a time series of transport through the channel for a much longer period. More specifically, we conducted surveys for multiple hours, covering both flood and ebb, to capture the variability of the total transport across the tidal channel (Fig. 1), which will then be analyzed with a regression to correlate with the vertically averaged flow velocity observed by a bottom-mounted ADCP in the center of the channel. We then use the regression coefficients obtained to calculate the total transport for the entire mooring period. We can then determine the impact of weather on the total transport through the tidal channel.

FIG. 2. Picture of the automated unmanned boat developed in the author's laboratory used in this study.

a. *The USV and surveys*

USVs are autonomous self-propelled platforms operating on the surface of water (e.g., Goudey et al. 1998; Roberts and Sutton 2006, 2012; Caccia et al. 2007; Codiga 2015; Liu et al. 2016) that can carry various loads with sensors and equipment for environmental surveys or monitoring. They can be used as educational tools and precision survey platforms for profiling the water column and measuring hydrographic parameters and bathymetry surveys (Vaneck et al. 1996; Brown et al. 2010). We have designed and developed several USVs for continuous surveys of current velocity profiles using an ADCP (Li and Weeks 2009; Weeks et al. 2011). The hull of the USV used in this study was aluminum (Fig. 2). The USV was equipped with a 1200-kHz ADCP mounted on a pole in front of the USV with the transducers facing downward and a high-resolution GPS (~0.25-m accuracy by a paid subscription in a designated area). The transducers of the ADCP were placed in water about 0.4 m below the surface. The USV uses two electric trolling motors, a laptop computer, a long-range (~10 km) wireless connection (to another computer on land), an autopilot system (written in Visual Basic), lead acid batteries, and a small generator. The control program allows for an unlimited number of predefined waypoints continuously. The USV has a cruise speed of up to 4.5 kt (2.25 m s^{-1}). The average offline distance (standard error) from the planned route was 0.97 m (Weeks et al. 2011).

On 19 September 2007, the first USV survey was conducted along a continuous radiator-shaped cross-channel route (Fig. 3a). This route has 10 segments laid across the channel, which can be used to calculate the along-channel transport, and 17 other segments, which

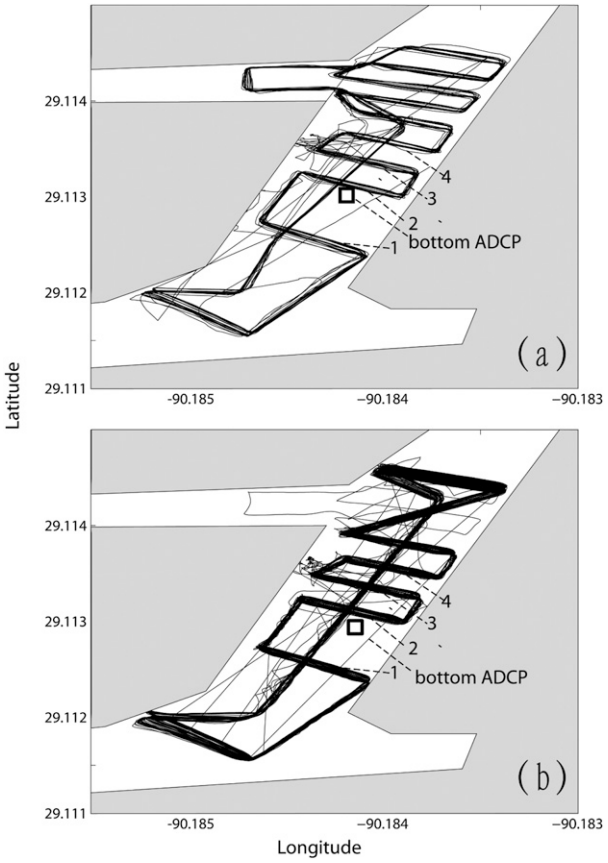

FIG. 3. Tracks of the USV for velocity measurements on (a) 19 Sep 2007 and (b) 8 Jan 2008. Location of bottom-mounted ADCP (square). Numbers 1–4 indicate the transect lines used for transport values for regression with data from the bottom-mounted ADCP.

do not provide the along-channel transport. An ADCP mounted on the USV was set up to record data at roughly 1-s intervals for velocity profiles at 0.25-m vertical intervals. Excluding the blanking distance on surface, the vertical profiles of the velocity vectors starting at 1.21 m below the surface down to the bottom were obtained. The data were recorded from 19:57:13 UTC 9 September, 2007 till 04:06:57 UTC 20 September.

On 8 January 2008, with the same setup, the second USV survey was conducted along a slightly modified route (Fig. 3b). This route has seven segments across the channel, which can be used to calculate the along-channel transport, and nine other segments, which do not provide the along-channel transport. The data were recorded from 22:31:14 UTC 8 January 2008 till 22:49:22 UTC 9 January. This gives about 24 h, 18 min of continuous time series data, covering roughly a whole tidal cycle (Fig. 3b).

Among the 10 (or 7 for the second cruise) cross-channel transects, only 4 of them close to the bottom-mounted ADCP were used (transects 14 in Figs. 3a,b). These four transects were identical for the two surveys, even though a few other transects were slightly modified. The other transects were more or less affected by the bifurcations and were thus not included in the analysis. During the 8-h, 10-min period of the first survey conducted on 19–20 September 2007, a total of 86 transect transport values from these four transects were obtained, averaging 21.5 repetitions per transect. During the 24 h, 18 min of the second survey conducted on 8–9 January 2008, a total of 89 repetitions for each of the four transects were made (a total of 356 transport values), among more than a total of 1500 times across the channel.

Figure 4 is the water depth averaged from the four transducers of the ADCP mounted on the USV. Figure 4b is an example of a surface flow velocity map from the first survey. There is a relatively deep hole of ~15 m at the T intersection of two channels (Fig. 4a). The water depth ranged between 2 and 15 m within the main channel.

b. *The moored ADCP data*

A 1200-kHz Teledyne RDI Workhorse ADCP was installed on a low-profile frame (SeaSpider) for bottom deployment. The instrument was deployed at a location roughly centered at the survey area between 31 October 2006 and 29 April 2008, covering the USV survey periods. The location of the ADCP is in the channel at a depth of ~6.5 m and in the middle of the route-covered area (Fig. 1) with coordinates 29.1133°N, 90.1841°W. A pressure sensor integrated with the ADCP allowed the recording of the water level at the same time when velocity profiles were saved. The vertical bins were set to be 0.2 m. The ensemble time intervals are mostly 900 s, except during the unmanned-boat surveys on 19–20 September 2007 and 8–9 January 2008, when it was set to 5 min, and during one short period of a few days, when it was unintentionally set to 1800 s. Over 99.96% of the data had time intervals of 900 s. The bottom-mounted ADCP data were quasi-regularly downloaded. There were 18 downloads of data, averaging a download every 29 days. There was a 0.7-day gap during one of the deployments. The only major data gap was a ~29-day period between 30 October and 28 November 2007, during which the instrument was maintained before redeployment. The rest of the data were quite continuous, with a few small gaps (one to two additional time steps or 15–30 min longer than the normal time step of 15 min). A total of 49 553 data records were saved. The total length of good data adds to about 515 days. During the first USV survey,

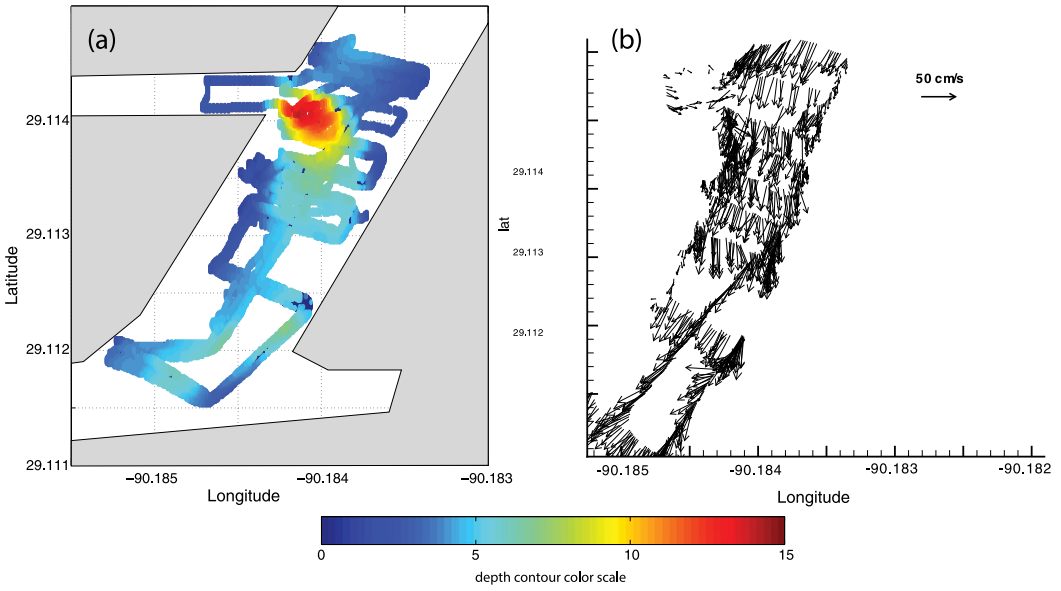

FIG. 4. (a) Mean water depth (m) measured on 19 Sep 2007. (b) Example of flow vectors measured from the USV. Depth is in reference to the local mean water level.

there were both positive (up to ~0.5 m s^{-1}) and negative (up to approximately −0.4 m s^{-1}) velocities from the bottom ADCP (Fig. 5a). During the second USV survey, the bottom-mounted ADCP measured flows in about a complete tidal cycle with velocity values ranging from −0.7 to 0.6 m s^{-1} (Fig. 5b).

To examine the characteristics of the vertical structure of the along-channel velocity time series, an empirical orthogonal function (EOF) analysis was done. The results show a dominant barotropic flow—the first mode has 98.2% of the variability with a quite uniform vertical structure. The second mode has only 0.47% of the variability, which shows a typical estuarine circulation structure with a top layer moving out of the channel and a bottom layer moving in (Fig. 6a). The third mode has only 0.13% of the variability, and each of the remaining modes has less than 0.08% of the variability, which can all be neglected. This provides justification for using the depth-averaged along-channel velocity to correlate with the total transport measured from the USV in this study. Figure 6b is an example of time series of velocity and water level; for convenience in visualizing the phase difference, the velocity and water level were normalized by reference values, so both are dimensionless (the velocity and water level were divided by 0.8 m s^{-1} and 0.4 m, respectively).

c. *Meteorological and water-level data*

Meteorological data including air pressure and wind velocity vectors at 6-min intervals were obtained from the National Data Buoy Center (NDBC) sites GISL1 (29.265°N, 89.958°W; Fig. 1) and BYGL1 (29.789°N, 90.42°W; Fig. 1). The reason why data from these two sites were used was the proximity of these stations to the study site and none of these sites had a complete dataset—some gaps existed. Data from these two sites are generally consistent. The meteorological data between 1 January 2006 and 30 April 2008 were mostly from the GISL1 site. The missing data was filled by that from the BYGL1 site. Wind and air pressure data were then interpolated into time series with the time interval of 1 h. Additional hourly water-level data were obtained from NOAA's tide gauge at Port Fourchon, Belle Pass, Louisiana, located at 29.1133°N, 90.1983°W (Fig. 1).

4. Analyses and discussion

a. *Regression for transport*

The USV ADCP–measured velocity data were first calibrated for misalignment and scaling (Joyce 1989). Each time the USV went across the channel, the velocity was integrated across the channel, with a linear extrapolation from 1.21 m below the surface to the surface and replacement of the near-bottom couple of data points by a linear interpolation to a bottom velocity of zero (to exclude errors caused by the sidelobe effect near bottom). The edge of the USV route was already very close to shore with shallow water because the unmanned boat can literally go to the shore with almost zero water depth (Weeks et al. 2011). A linear extrapolation was made to

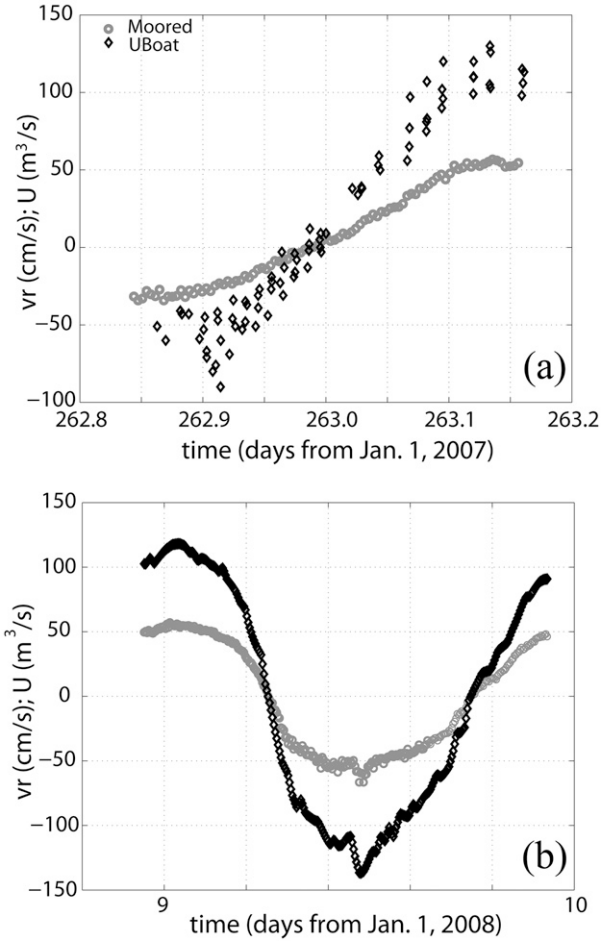

FIG. 5. (a) Depth-averaged velocity from the bottom-mounted ADCP and transport values from the USV for the first survey. (b) Depth-averaged velocity from the bottom-mounted ADCP and transport values from the USV for the second survey.

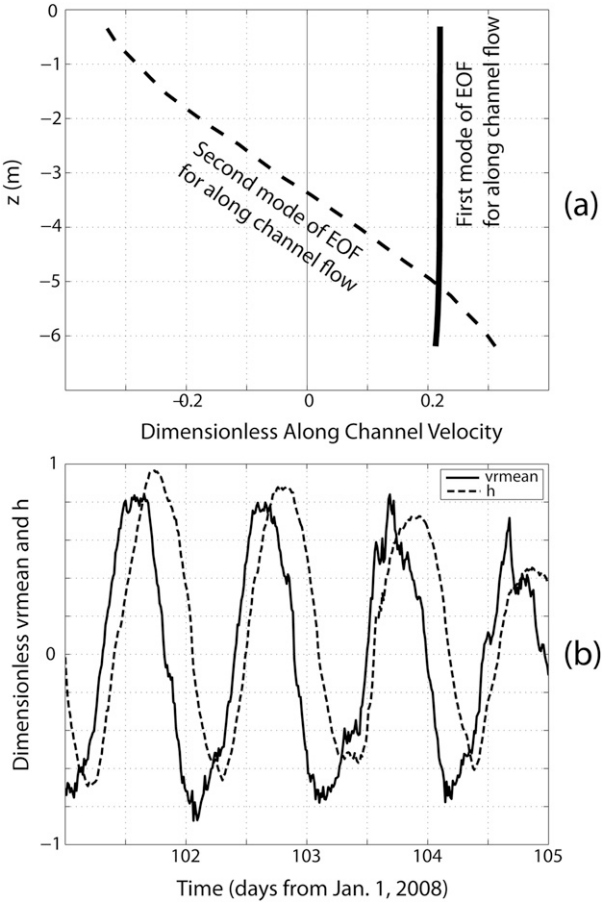

FIG. 6. (a) First mode (98.2%) and second mode (0.47%) of the EOF for the vertical structure of the along-channel horizontal velocity component. (b) Example time series of normalized (dimensionless) water level and depth-averaged along-channel velocity.

include values near the side boundaries in the integration for the total cross-channel transport. These transport values were then interpolated onto the times of the bottom-mounted ADCP (at 5-min intervals).

The mean velocity from the bottom-mounted ADCP and the transport from USV ADCP appear to follow each other when plotted on the same graph (but with different units: cubic meter per second vs centimeter per second; Figs. 5a,b). Before examining the correlation between depth-averaged flow velocity measured from the bottom-mounted ADCP with the transport measured from the USV ADCP, the flow data from bottom-mounted ADCP were first checked to find the principal components, so we can rotate the coordinate system to align with the major along-channel velocity. For the data we obtained, the coordinate system was rotated −8° (negative means clockwise; Figs. 7a,b). After interpolating the data from the USV ADCP onto the time of the bottom-mounted ADCP data, the following regression was attempted:

$$U = \alpha \overline{v_r} + \beta \tag{1}$$

in which U ($\mathrm{m^3\,s^{-1}}$) is the transport measured from the USV ADCP, $\overline{v_r}$ ($\mathrm{cm\,s^{-1}}$) is the depth-averaged along-channel velocity from the bottom ADCP. For the first survey (19 September 2007), the regression coefficients are $(\alpha, \beta) = (2.1625, -0.6875)$, in which both are dimensional, such that α has a unit of $100\,\mathrm{m^2}$ and β has a unit of a cubic meters per second. The 95% confidence interval for α is (2.0643, 2.2607); the 95% confidence interval for β is (−3.4939, 2.1189), and the R^2 is 0.9630.

For the second survey (8–9 January 2008), the regression coefficients are $(\alpha, \beta) = (2.0850, -1.5104)$, and $R^2 = 0.9963$. The 95% confidence interval for α is

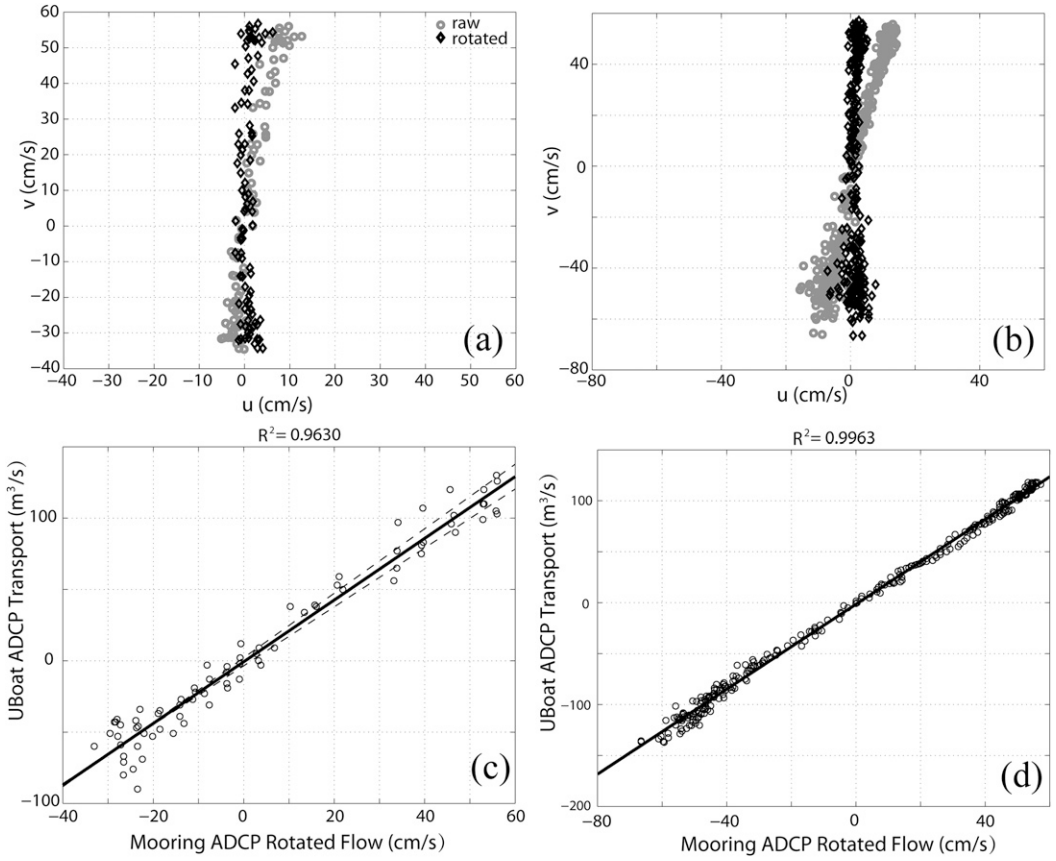

FIG. 7. (a) Raw along-channel depth-averaged velocity and rotated version for the first survey. (b) Raw along-channel depth-averaged velocity and rotated version for the second survey. (c) Correlation between depth-averaged velocity from the bottom-mounted ADCP and transport values from the USV for the first survey. (d) Correlation between depth-averaged velocity from the bottom-mounted ADCP and transport values from the USV for the second survey.

(2.0700, 2.0999); the 95% confidence interval for β is (−2.1291, −0.8916). If the data from both survey are combined, then a single unified regression yields the regression coefficients of $(\alpha, \beta) = (2.0800, -1.9954)$, and $R^2 = 0.9863$. The 95% confidence interval for α is (2.0419, 2.1181); the 95% confidence interval for β is (−3.4021 to 0.5887). Obviously, the regression shows a quite clean linear correlation between the two datasets (Figs. 7c,d).

Applying the regression coefficients to the entire time series of depth-averaged velocity from the bottom-mounted ADCP, the integrated along-channel volume transport of water for 515 days is obtained (Figs. 8a,b). It can be seen that the transport has an order of magnitude of 100–150 $m^3 s^{-1}$, with clear diurnal tidal signals and spring–neap variations. Underneath the apparently trivial daily oscillation is the weather-induced low-frequency or subtidal transport variations. To analyze the weather effect, a 40-h Butterworth low-pass filter (Butterworth 1930) was applied. This is a filter that has a smooth and uniform pass band and a relatively clean cutoff, which is widely used in physical oceanography (Moeller et al. 1993; Dingler et al. 1993; Keen 2002; Emery and Thomson 2004; Feng and Li 2010; Li et al. 2011a; Li 2013). Figure 8c is an example of the low-pass filtered transport. By comparing the timing of maximum outward transport with weather maps, linkages between the abnormal variations in transport and severe weather can be established. This is discussed in more detail after the next section.

b. *Fourier and harmonic analysis*

A Fourier analysis was performed for the time series data for both the water level (Fig. 9a) and transport (Fig. 9b). The spectra showed consistent results for major peaks at tidal frequencies: the vertical dashed lines of Figs. 9a,b indicate the frequencies of eight major tidal constituents (M_1, O_1, P_1, S_1, K_1, N_2, S_2, and M_2).

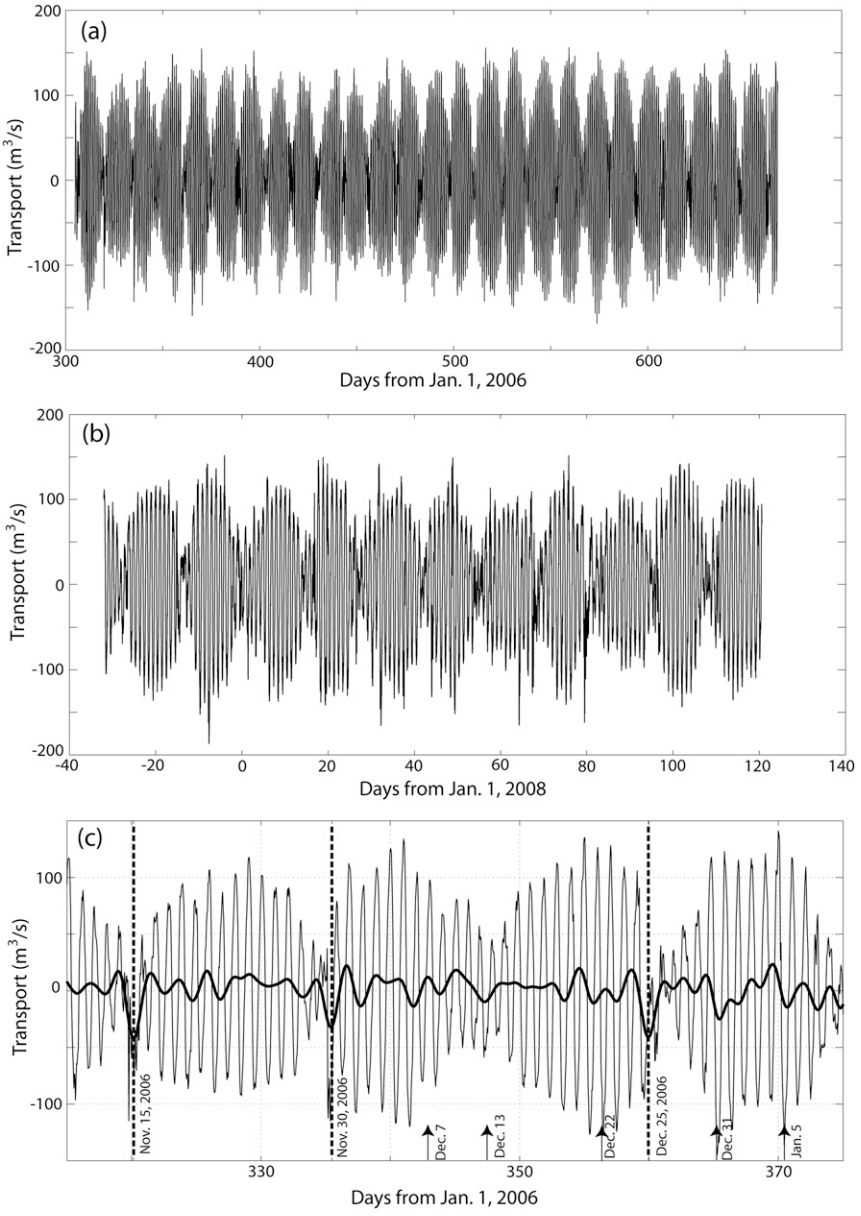

FIG. 8. Time series of transport calculated from the correlation with the USV measurements. (a) Transport before the 29-day gap or before 30 Oct 2007. (b) Transport after the 29-day gap or after 28 Nov 2007. (c) Segment of zoom-in time series before the 29-day gap.

The relatively large values at low frequencies are responses from the weather.

A quick check of the water level and the depth-averaged along-channel velocity reveals that they appear to be out of phase; that is, a maximum water level would follow the maximum inward flow velocity, or the phase of flow leads that of water elevation (Fig. 6b). For a standing wave, the phase difference would be 90°. In this case, however, the maximum flow occurs after the water elevation reaches the mean level during rising tide, so the water level reaches its maximum sooner than that with a 90° phase difference (Fig. 6b). This should be caused by friction in the shallow water and under strong currents. The exact phase difference can be calculated with the harmonic analysis.

To quantify the harmonic constants for tidal elevation and velocity, the following eight major tidal constituents are selected for a harmonic analysis: M_2, S_2, N_2, K_1, O_1,

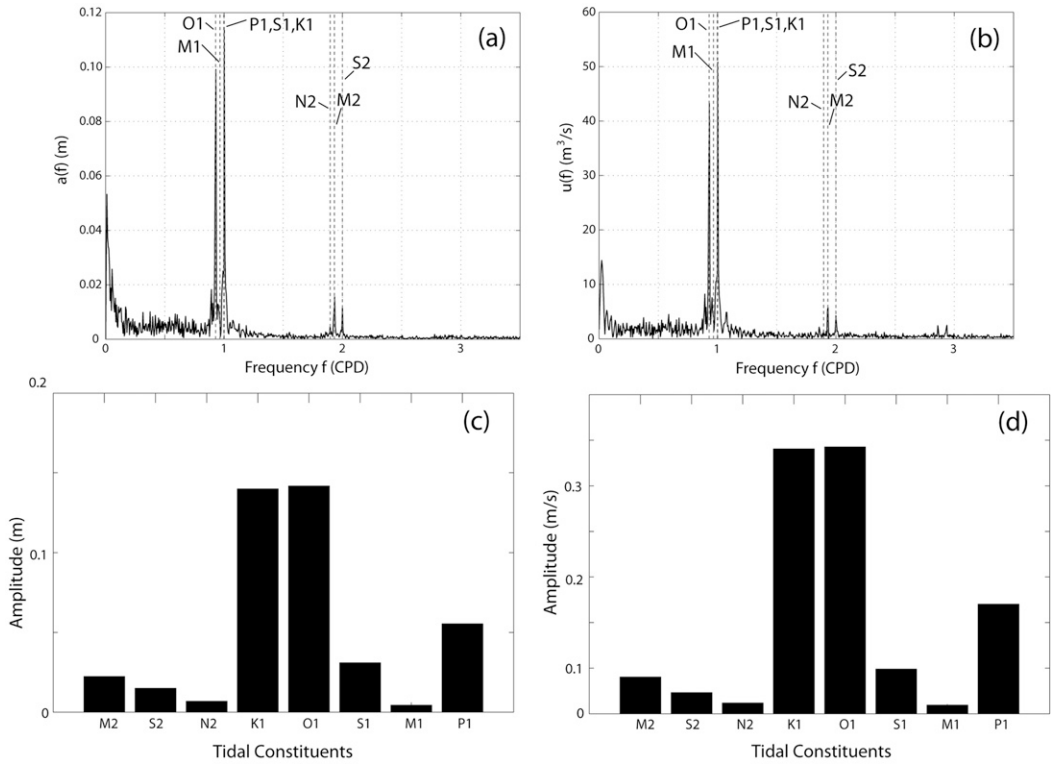

FIG. 9. Fourier transform using FFT for (a) the water elevation and (b) the depth-averaged along-channel velocity from the bottom-mounted ADCP. Amplitude for the eight tidal constituents for (c) water level and (d) depth-averaged velocity. Units here are the same as for the FFT for the original data. For convenience the FFT results were multiplied by $2/N$, in which N is the total length of record of the data; factor of 2 is for the one-sided spectrum, so we do not need to use negative frequency.

S_1, M_1, and P_1 tides, consistent with what was observed from the spectra (Figs. 9a,b). The method was based on and modified from Li et al. (2000). It used the same convention as NOAA and as described in Boon (2004). The method was verified with NOAA's published harmonic constants (Li et al. 2017). The time is in UTC. Harmonic analysis results show that the dominant tidal constituents for both water-level and velocity variations are K_1 and O_1, followed by P_1 and S_1. The amplitudes of K_1, O_1, P_1, and S_1 diurnal tides are 0.14, 0.14, 0.06, and 0.03 m, respectively, whereas the semidiurnal tidal amplitudes of M_2, S_2, and N_2 are 0.02, 0.02, and 0.01 m, respectively. The amplitudes of K_1, O_1, P_1, and S_1 diurnal along-channel tidal velocity are 0.29, 0.29, 0.12, and 0.05 m s^{-1}, respectively. The semidiurnal along-channel tidal velocity amplitudes of M_2, S_2, and N_2 are 0.04, 0.02, and 0.01 m s^{-1}, respectively (Table 1; Fig. 9).

c. *Weather impact*

The low-pass filtered transport shows some fluctuations but with apparent episodes of relatively large outward (with negative sign) transport values from time to time. Occasionally, there were some relatively large inward (positive) transports. A thorough examination of

TABLE 1. Harmonic analysis results, where h is water depth, v is demeaned along-channel depth-averaged velocity, phase_h is phase for h, and phase_v is phase for v.

Frequency	M_2	S_2	N_2	K_1	O_1	S_1	M_1	P_1
h (m) ($\bar{h}$ = 6.64 m)	0.02	0.02	0.01	0.14	0.14	0.03	0.00	0.06
v (m s^{-1})	0.04	0.02	0.01	0.29	0.29	0.05	0.01	0.12
phase_h (°)	2.6	166.7	141.2	32.6	210.8	250.6	156.5	47.6
phase_v (°)	270.9	121.7	63.0	336.4	151.6	214.1	162.6	359.6
dphase (°)	−268.3	45.1	78.2	−303.8	59.3	36.5	−6.1	−312.0

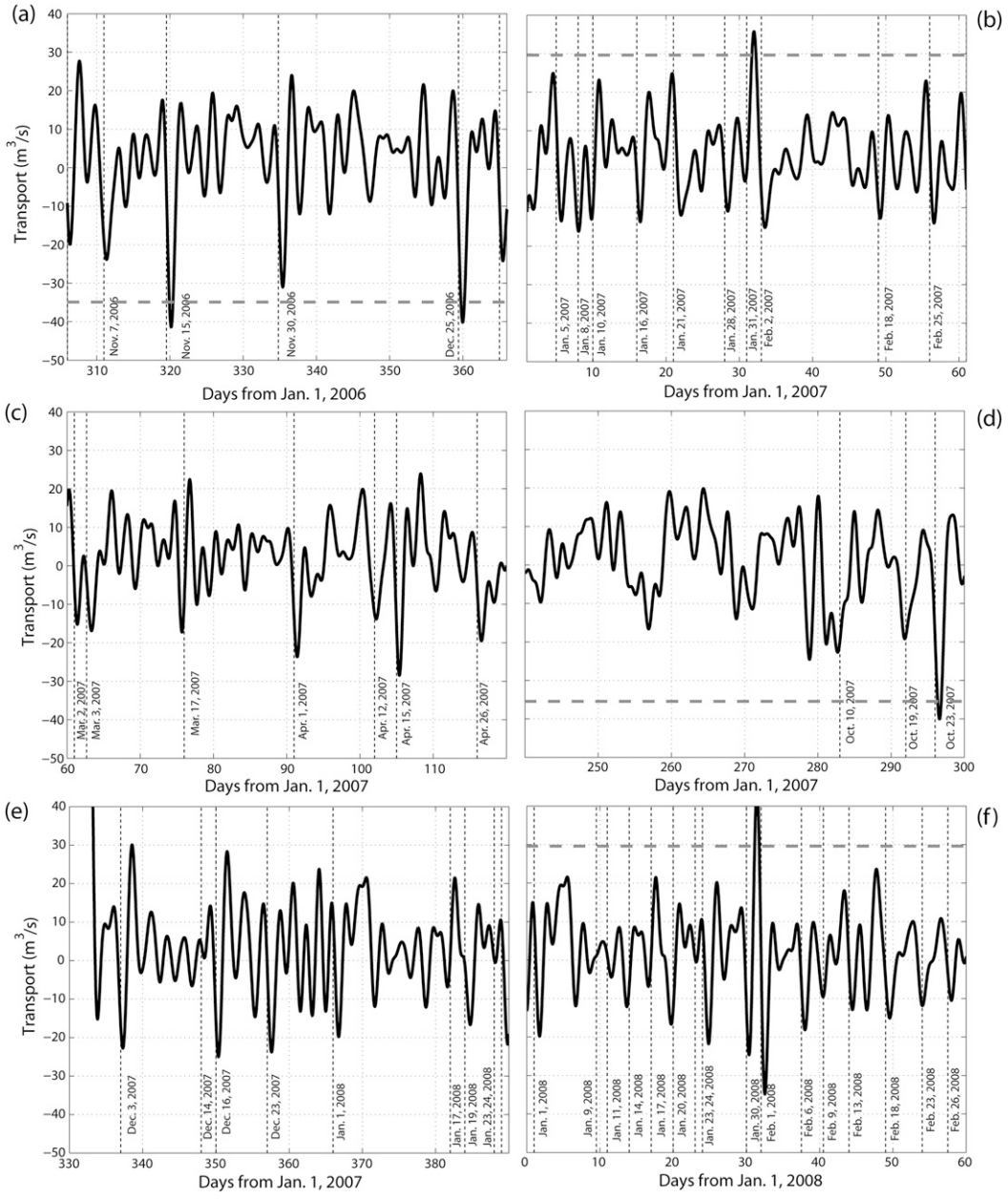

FIG. 10. Low-pass filtered transport time series calculated using the regression between the depth-averaged flow velocity and the transport measured from the unmanned boat. Time of an atmospheric frontal passage (vertical dashed lines). Thresholds for extreme events discussed in this paper (thick dashed horizontal lines).

all weather maps for the entire study periods reveals that most of these episodes of relatively large oscillations in total transport appear to be associated with severe weather, mostly cold fronts (e.g., Roberts et al. 1989; Walker and Hammack 2000; Feng and Li 2010; Li 2013; Kupchik 2014; Li and Chen 2014; Lin et al. 2016), and sometimes coastal warm fronts. More specifically, the following dates were found to have a major cold front passage: 15 and 30 November and 25 December 2006, 15 April and 23 October 2007, and 7 and 19 March 2008 (Figs. 10, 11). There were many minor cold front passages, such as those on 7, 13, 22, and 31 December 2006; 5, 16, and 21 January; 18 and 25 February; and 2 March 2007. A more complete list of cold and warm fronts can be found in Table 2—a total of 76 cold or warm fronts were identified during the study period, most of which were cold fronts. The timing listed in Table 2 was from the weather maps with the front having the closest

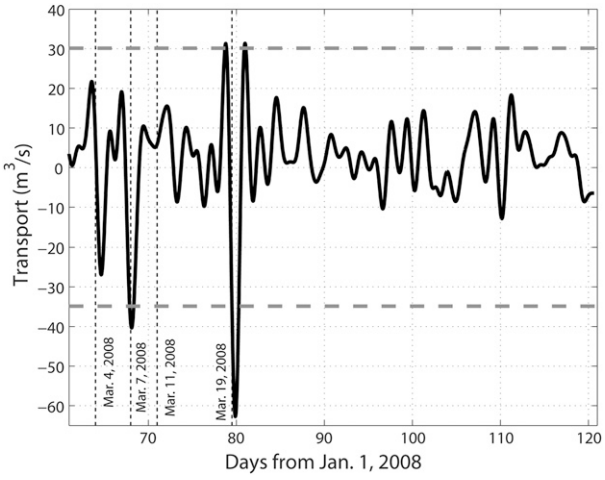

FIG. 11. Low-pass filtered transport time series (continued from Fig. 9) calculated using the regression between the depth-averaged flow velocity and the transport measured from the unmanned boat. Time of an atmospheric frontal passage (vertical dashed lines). Thresholds for extreme events discussed in this paper (thick dashed horizontal lines).

proximity to the study site. In the following subsections, we will discuss seven of the largest of the 76 processes. These seven events all produced a low-pass filtered transport with a magnitude of 30 $m^3 s^{-1}$ or more for warm front events and 35 $m^3 s^{-1}$ (with negative sign) or more for cold front events. The use of 30 and 35 $m^3 s^{-1}$ as thresholds (Figs. 10, 11) is mainly for convenience, so the discussion will focus only on a few relatively large cold and warm front events.

1) COLD FRONT, 15 NOVEMBER 2006

A low air pressure was centered in northern Texas at 0000 UTC 15 November 2006. A couple of cold fronts were pushing from its north. Another cold front associated with this low pressure center extended from Southern California through Arizona and New Mexico to northern Texas, with its length estimated to be ~1500 km. A stationary front associated with this low pressure center extended from northern Texas toward the southeast to southeastern Louisiana. In the next 12 h, the low pressure changed to an extratropical cyclone and slowly moved to east through southern Oklahoma, during which the stationary front turned into a warm front, drawing warm and moist air from the Gulf of Mexico. The originally east–west-oriented cold front started to turn counterclockwise and became more and more north–south oriented. At 1500 UTC, the extratropical cyclone reached its mature stage and its cold front was crossing western Louisiana coastline. At 1800 UTC, the low pressure center of the cyclone reached the southwest corner of Tennessee and the cold front almost reached the study site in southern Louisiana (Fig. 12a). The postfrontal passage wind was strong, which reached 20–40 kt on the ground in much of coastal Texas (Fig. 12a). The resultant low-pass filtered outward transport was greater than 40 $m^3 s^{-1}$.

2) DOUBLE COLD FRONTS, 25 DECEMBER 2006

At 0000 UTC 24 December, a cyclone formed at the Texas–Mexico border and moved eastward and northeastward in the next 24 h. The center of this cyclone and the northern tip of the cold front quickly passed southern Louisiana by 0300 UTC 25 December (Fig. 12b). At this time, a second front can be seen moving toward the area covering Iowa, Missouri, Oklahoma, and Texas, with a length of ~2000 km. These two fronts came through the area back to back. Even though none of these fronts were very strong, the combined force produced a significant outward flow of ~40 $m^3 s^{-1}$ (Fig. 10a), comparable to the case discussed above by the single cold front on 15 November (Fig. 10a).

3) WARM FRONT, 1 FEBRUARY 2007

There was a large-scale warm front on 1 February 2007. It was shown on weather maps after the passing of an earlier cold front on the East Coast followed by an anticyclone (high atmospheric pressure at sea level) that was centered on Kentucky at 1500 UTC 31 January 2007, with a diameter of ~2500 km. This facilitated a sea level southerly wind from the Gulf of Mexico landward. As the high pressure center moved eastward, warm air was drawn northward, and the warm front moved northward toward the coastline. The ground-level wind was easterly. This continued for another 15 h, when the warm front crossed the southeastern Louisiana coast and the study area (Fig. 12c). For the following 9 h, the front basically stalled and became a stationary front. In the next 3 h, the front reformed and started to move again as a cold front as a >1800-km line at 1800 UTC 1 February. During much of this period, coastal Louisiana had easterly, or southeasterly winds, leading to a pileup of water on the coast, causing a net inward transport into the channel with a magnitude of ~35 $m^3 s^{-1}$ (Fig. 10b).

4) COLD FRONT, 23 OCTOBER 2007

On 21 October 2007, after a cold front associated with an extratropical cyclone centered at eastern Canada moved cross the Eastern Seaboard, a sea level air pressure trough extending ~3000 km to the south was pushed offshore. A high pressure system occupied much of the eastern states; it moved offshore followed by a large-scale curved cold front extending more than 3000 km from the Great Lakes area to northern Mexico.

TABLE 2. Cold/warm front occurrence time (UTC). Y: year. M: month. D: day. H: hour. Boldface lines correspond to the events discussed in detail.

	Start time				End time					Start time				End time			
No.	Y	M	D	H	Y	M	D	H	No.	Y	M	D	H	Y	M	D	H
1	2006	11	1	0000	2006	11	2	0600	39	**2007**	**10**	**22**	**1200**	**2007**	**10**	**23**	**1200**
2	2006	11	6	1800	2006	11	7	1500	40	2007	11	29	0600	2007	11	29	2100
3	2006	11	10	2100	2006	11	11	1800	41	2007	12	3	0000	2007	12	3	1200
4	**2006**	**11**	**15**	**0900**	**2006**	**11**	**16**	**0000**	42	2007	12	5	2100	2007	12	6	1200
5	2006	11	30	1200	2006	12	1	0600	43	2007	12	13	0300	2007	12	14	2100
6	2006	12	6	2100	2006	12	7	1200	44	2007	12	15	1500	2007	12	16	0300
7	2006	12	12	1200	2006	12	13	0300	45	2007	12	20	1800	2007	12	21	0900
8	2006	12	22	0600	2006	12	23	0300	46	2007	12	22	1800	2007	12	23	0900
9	**2006**	**12**	**24**	**1500**	**2006**	**12**	**25**	**0300**	47	2007	12	26	1800	2007	12	27	0900
10	2006	12	30	0900	2006	12	31	1200	48	2007	12	28	0900	2007	12	29	0900
11	2007	1	4	1200	2007	1	5	1200	49	2008	1	1	0000	2008	1	1	0900
12	2007	1	7	0600	2007	1	8	0300	50	2008	1	8	1500	2008	1	9	1500
13	2007	1	9	1200	2007	1	9	2100	51	2008	1	10	1200	2008	1	11	1200
14	2007	1	15	0300	2007	1	16	0600	52	2008	1	16	1200	2008	1	17	0600
15	2007	1	21	0600	2007	1	22	1200	53	2008	1	19	0900	2008	1	19	1800
16	2007	1	27	1500	2007	1	28	0300	54	2008	1	22	1800	2008	1	23	1500
17	2007	1	27	2100	2007	1	29	0000	55	2008	1	26	0300	2008	1	26	1800
18	**2007**	**2**	**1**	**1500**	**2007**	**2**	**2**	**0000**	56	**2008**	**1**	**29**	**1800**	**2008**	**1**	**30**	**0600**
19	2007	2	4	1200	2007	2	5	1800	57	**2008**	**1**	**31**	**1800**	**2008**	**2**	**1**	**0300**
20	2007	2	8	1800	2007	2	9	1200	58	2008	2	6	0000	2008	2	6	1500
21	2007	2	9	1800	2007	2	10	0600	59	2008	2	7	2100	2008	2	8	1200
22	2007	2	13	0900	2007	2	14	0300	60	2008	2	8	2100	2008	2	10	0000
23	2007	2	17	1200	2007	2	18	0000	61	2008	2	12	1200	2008	2	13	0900
24	2007	2	22	0900	2007	2	23	0900	62	2008	2	17	0300	2008	2	18	0000
25	2007	2	24	2100	2007	2	25	1800	63	2008	2	17	1800	2008	2	18	0900
26	2007	3	1	1200	2007	3	2	0600	64	2008	2	22	0300	2008	2	23	0300
27	2007	3	3	0300	2007	3	3	1500	65	2008	2	26	0300	2008	2	26	1500
28	2007	3	16	0300	2007	3	16	1800	66	2008	3	3	1500	2008	3	4	0900
29	2007	4	4	0600	2007	4	5	0000	67	**2008**	**3**	**7**	**0000**	**2008**	**3**	**7**	**0900**
30	2007	4	11	0900	2007	4	12	0600	68	2008	3	10	2100	2008	3	11	1800
31	2007	4	14	0600	2007	4	15	0300	69	2008	3	15	0900	2008	3	16	0600
32	2007	4	18	0600	2007	4	18	1500	70	**2008**	**3**	**19**	**0300**	**2008**	**3**	**19**	**1500**
33	2007	4	20	0300	2007	4	20	1500	71	2008	3	22	0600	2008	3	23	0900
34	2007	4	26	0000	2007	4	26	1800	72	2008	4	1	1500	2008	4	2	1500
35	2007	9	15	0300	2007	9	16	0900	73	2008	4	4	1200	2008	4	5	1800
36	2007	9	28	090	2007	9	29	0900	74	2008	4	11	0900	2008	4	12	1200
37	2007	10	9	0000	2007	10	10	0900	75	2008	4	18	0900	2008	4	19	0900
38	2007	10	18	1800	2007	10	19	1500	76	2008	4	27	1500	2008	4	28	0900

Meanwhile, the central Gulf of Mexico had a warm front of ~1400 km, drawing southerly winds to the southern states (covering from Texas to the eastern coast of Florida). By 1500 UTC 22 October, the cold front quickly moved to the northwestern corner of Louisiana, extending from Canada to Mexico for more than 3000 km, while the warm front pushed onto land, covering from the Louisiana border to the eastern coast of Florida. For the next 3 h, the southern portion of the front moved only to western Louisiana. At 0300 UTC 23 October, the front was just about to pass the study site (Fig. 12d). In the next 3 h, the front barely passed the study site. At 0900 UTC 23 October, the front moved to the southern tip of the bird-foot delta. It is probably this slow-moving cold front and associated westerly winds that lowered the coastal water through the Ekman effect that caused the relatively large outward transport of approximately $-40\,m^3\,s^{-1}$ (Fig. 10d).

5) COLD–WARM–COLD FRONT COMBINATION, 30 JANUARY–1 FEBRUARY 2008

It is very interesting that there was a cold–warm–cold front combination event during the study period. It started 29–30 January 2008, when a roughly north–south-oriented cold front extending from Canada to southern Texas swept through Louisiana. At about

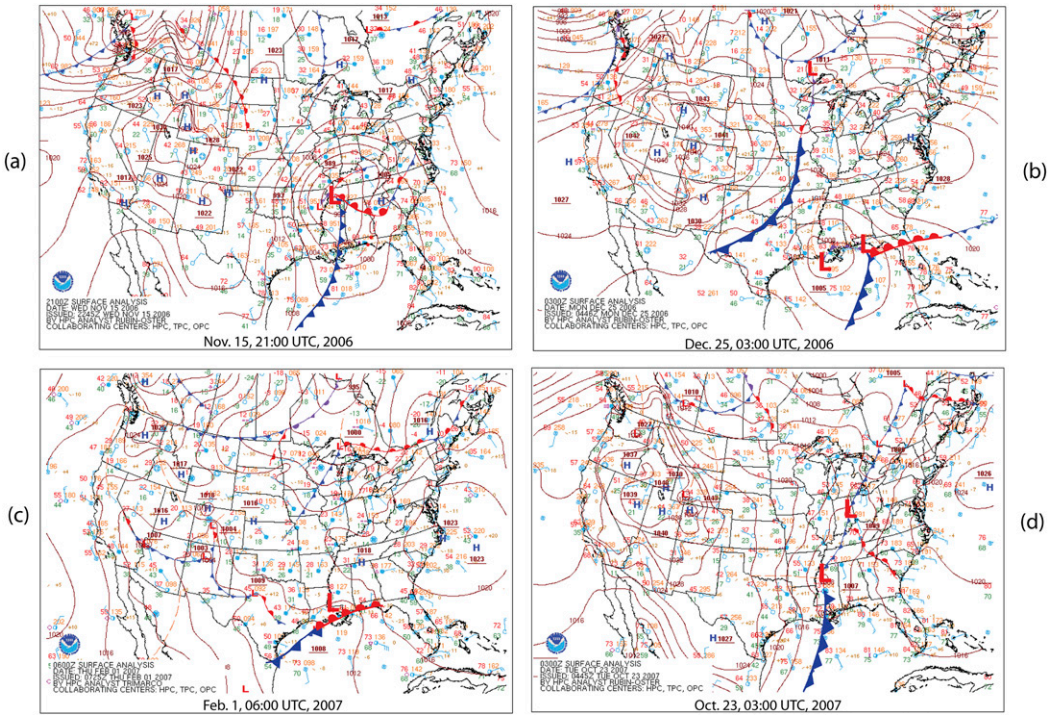

FIG. 12. Weather maps from NOAA for the selected extreme weather associated with atmospheric frontal passages of the study area for (a) 15 Nov 2006, (b) 25 Dec 2006, (c) 1 Feb 2007, and (d) 23 Oct 2007.

0300 UTC 30 January, the front was oriented northeast–southwest at about 45° to the coastline, passing the study site. It moved relatively quickly—in 3 h it already moved cross Florida. This is contrary to the slow-moving cold front of 23 October 2007, discussed above. At 0600 UTC 30 January, the center of high pressure following the front moved to the Texas–Arkansas–Louisiana border, while the southern portion of the cold front moved into the Gulf of Mexico. In the next 12 h, the northern portion of the cold front over the mainland crossed the Eastern Seaboard into the Atlantic Ocean, while the southern portion of the front moved farther toward the south of the Gulf of Mexico and gradually lost its momentum and became a stationary front (1800 UTC 30 January). Starting from this point, the front inside the Gulf of Mexico became a warm front and gained its strength, apparently pushed by the marine tropical air mass. At 0900 UTC 31 January, this warm front had already been well developed, covering the entire northern Gulf of Mexico for over 1800 km. At 1200 UTC 31 January, the warm front had advanced to the southern Louisiana coast (Fig. 13a). At 1800 UTC 31 January, the warm front had pushed beyond central Louisiana, while its western portion had already interacted with an advancing cold front and formed an occluded front and a low pressure centered at the Texas–Louisiana–Arkansas border. In the next 6 h, the low pressure center moved southeast when the cold front crossed the study site (Fig. 13b). During the warm front, wind was persistently easterly or southeasterly, pushing water onshore with either direct wind forcing or Ekman transport. This resulted in the largest low-pass filtered inward transport of greater than $40\,m^3\,s^{-1}$ in our entire 515 days of data. The two cold fronts both prior to and after the passage of the strong warm front worked in sequence in producing the outward transport of approximately -25 and $-35\,m^3\,s^{-1}$, respectively (Fig. 10f).

6) COLD FRONT, 7 MARCH 2008

On 6 March 2008, a cold front was approaching Louisiana from the northwest. The front was moving slowly and even stalled at one time (i.e., at 1500–1800 UTC 6 March). At the same time, a warm front developed in the central region of the Gulf of Mexico, moving north-northeastward and converging with the southeastward-moving cold front. The two fronts met at about the study site where a low pressure was formed (0600 UTC 7 March; Fig. 13c). Subsequently, the low pressure moved offshore with the cold front followed by a northwesterly wind at the study site.

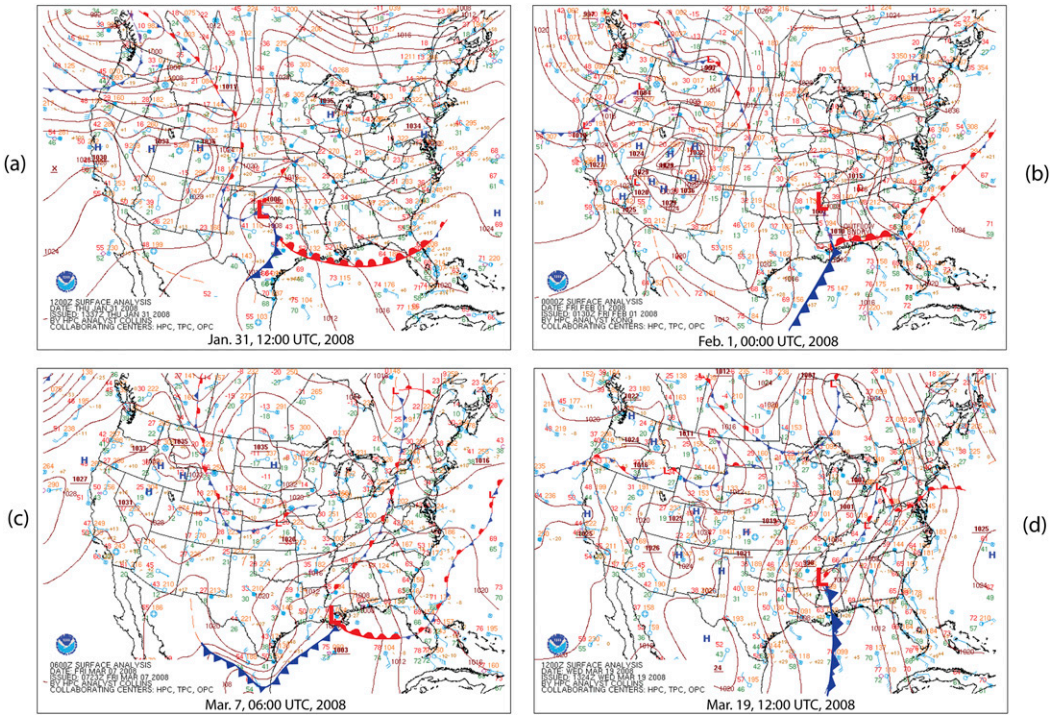

FIG. 13. Weather maps from NOAA for the selected extreme weather associated with atmospheric frontal passages of the study area for (a),(b) 31 Jan–1 Feb 2008, (c) 7 Mar 2008, and (d) 19 Mar 2008.

This was another rather interesting event not just because it was producing a strong outward transport of $40\,m^3\,s^{-1}$ (Fig. 11) at the study site, but because it was reported to have produced some unique series of solitary waves of ~1 m in height (Sheremet et al. 2016). Sheremet et al. (2016) originally aimed to study wave dissipation in the muddy environment on the southern Louisiana coast. They deployed an array of instruments with pressure sensors sampling at 2 Hz, which happened to have captured the event. The instruments were deployed northwest of the Trinity Shoal and south of Atchafalaya Bay. The instruments recorded a cluster of cnoidal waves or solibore or what they believed to be a disintegrating wave train as a KdV solution, proceeded by a solitary wave. These waves had an order of magnitude of about 1 m in height and a 20-s time scale. By coincidence, a few instruments were also deployed by a group of researchers at Louisiana State University at the Wax Lake delta at 29.472°N, 91.478°W, which included pressure sensors and ADCPs sampling at 1 Hz. They were deployed just hours before the event on 6 March 2008 and were retrieved a month later on 5 April. The data from this effort not only showed the train of solitary waves on 7 March but also on 19 March (the next case). The latter case was not reported in Sheremet et al. (2016). To avoid complicating the discussion, the data from the Wax Lake delta will not be presented and discussed here.

7) WARM–COLD FRONT, 19 MARCH 2008

At 0000 UTC 17 March 2008, a couple of high pressure systems were centered at Lake Superior and at the border of the Carolinas, producing warm and moist air landward at the Louisiana and Texas coast from the south and southeast together with a long warm front of ~2000 km cross the Louisiana and Texas coasts, respectively. Wind at the Louisiana coast reached at least 20 kt (1800 UTC 17 March). This condition persisted for another 18 h, when the high pressure system center barely moved away from Virginia, facilitating the constant drawing of air from the Gulf of Mexico with the southeasterly wind at the Louisiana coast. At the same time (1200 UTC 18 March), a cold front was approaching with a large-scale high pressure system from the northwest. From 1800 UTC 18 March through 0000 UTC 19 March, the center of high pressure moved offshore. As the following high pressure system from the west pushed eastward, the pressure contours were converging and the wind increased. Subsequently, a couple of low pressure centers formed in eastern Texas and central Arkansas. The cold front moved across the study site at ~1200 UTC 19 March, almost perpendicular to

the coastline. As the cold front swept through the southern states of Louisiana, Mississippi, Alabama, and Florida in that order, the postfrontal northerly and northeasterly winds kept strong (~20 kt) at the coast of Louisiana for the next 27 h. Apparently, the earlier warm front and high pressure system associated with southerly winds produced the relatively large inward transport of $\sim 30\,m^3\,s^{-1}$ at the study site. The cold front passage brought persistent strong northerly and northeasterly winds that induced the largest outward transport of $\sim 60\,m^3\,s^{-1}$ (Fig. 11) for the entire 515 days of the observation period (Fig. 13d). The relaxation after the strong post–cold frontal wind caused the rebound and the inward transport of $\sim 30\,m^3\,s^{-1}$.

d. Correlation and regression analysis

To examine the effect of weather, we use the low-pass filtered (with the 40-h Butterworth filter) or bandpass filtered data within the weather band [0.14–0.33 cpd (cycle per day), corresponding to ~3–7 days, which are the cold front return periods; Roberts et al. 1989]. Correlation coefficients between the low-pass filtered meteorological parameters (east wind components, north wind components, and air pressure) and the water elevation at the Port Fourchon tide gauge were calculated. Similar correlations for the weather band were also calculated. All these calculations were performed for the entire periods. The results show that air pressure and the low-pass filtered water level are inversely correlated, with a correlation coefficient of −0.63. North winds and the low-pass filtered water level are positively correlated, but the correlation coefficient is small (0.24). East winds have a larger linear correlation with the low-pass filtered water level. However, within the weather band, the correlation coefficient between air pressure and water level is −0.82, indicating that the weather band has a higher correlation with the water level in that band. Within the weather band, the correlation of the water level with the north wind component also sees some increase in magnitude (0.41). The linear correlation is of course not proof of any linear or nonlinear dynamical relationship among variables. This is especially true considering the process of having a phase delay between forcing and response. Nevertheless, the correlation is an indication that there is a linkage between the atmospheric weather system passage and the subtidal ocean response.

e. Coherence analysis

To complement the time domain correlation coefficient estimate, an analysis in frequency domain is also done: the magnitude-squared coherence (MSC) function is calculated. This is aimed at the statistical relationship (correlation coefficient) in the frequency domain between forcing and response. The MSC is a function of frequency f, ranging between 0 and 1, defined by

$$\gamma_{xy}^2(f) = \frac{|S_{xy}(f)|^2}{S_{xx}(f)S_{yy}(f)}, \tag{2}$$

in which x and y represent the forcing and response time series, respectively; $S_{xx}(f)$, $S_{yy}(f)$, and $S_{xy}(f)$ are the spectra of x and y, and the cross spectrum of x and y, respectively. Here the MSC function $\gamma_{xy}^2(f)$ is calculated based on Welch's averaged periodogram method (Welch 1967).Using the 40-h low-pass filtered data, the MSC function is obtained for pairs of variables (i.e., transport and air pressure, transport and east wind velocity component, or transport and north wind velocity component). Since the 40-h low-pass filter is equivalent to a cutoff frequency of 0.6 cpd, the MSC as a function of frequency is useful for frequencies lower than 0.6 cpd. It is found that the mean MSC values between the water transport and the meteorological parameters are ~0.48 (between transport and air pressure), 0.35 (between transport and north wind), and 0.40 (between transport and east wind) (Table 3). These values all increase for the weather band: 0.54 (between transport and air pressure), 0.38 (between transport and north wind), and 0.46 (between transport and east wind). The maximum MSC values are all above 0.7, that is, 0.81 (between transport and air pressure), 0.71 (between transport and north wind), and 0.84 (between transport and east wind). Note that these maximum values all occur inside the weather band, that is, 3.8 days (between transport and air pressure), 3.3 days (between transport and north wind), and 3.3 days (between transport and east wind), with an average of 3.4 days (Table 3). In contrast, all the minimum MSC values occur outside of the weather band. This supports the idea and is consistent with the results of an analysis that the low-pass filtered transport is mainly caused by the atmospheric cold fronts.

f. Mechanism discussion

From Figs. 10 and 11 it is obvious that the timing of frontal passages and that of the minimum or maximum of the transport coincide with each other; that is, the minimum (maximum) transport occurred at the time of the passage of a cold (warm) front. This is what we call the "immediate response" or the transport (as well as the water level and velocity) and air pressure anomaly are roughly in phase for the low-pass filtered time series because the timing of these frontal passages is determined by the frontal lines, where the air pressure reaches its

TABLE 3. Magnitude-squared coherence with transport.

MSC	Air pressure	North wind	East wind	Unit	Note
Mean	0.4751	0.3498	0.3985		All band[a]
Mean	0.5389	0.3816	0.4594		Weather band[b]
Max	**0.8147**	**0.7088**	**0.8412**		All band[a]
Max	0.8147	0.7088	0.8412		Weather band[b]
Min	0.0472	0.0104	0.0519		All band[a]
Min	0.1585	0.0897	0.1548		Weather band[b]
fmax	**0.2636**	**0.3046**	**0.3046**	cpd	
Tmax	**3.7936**	**3.283**	**3.283**	Day	
Mean(fmax)		0.2909		cpd	
Mean(Tmax)		3.4		Day	

[a] All band: 0–0.6 cpd in frequency, or ~40 h to infinity in period.
[b] Weather band: 0.14–0.33 cpd in frequency, or ~3–7 days in period.

minimum for cold fronts. This is verified by the correlation discussed earlier.

For the cold front cases, prior to the frontal passage, wind is usually onshore (southerly, southwesterly, or southeasterly). After the frontal passage, wind is usually offshore (northerly, northwesterly, or northeasterly). For the warm front cases, wind is usually onshore first and reaches its maximum at the (warm) frontal passage, after which the cold front connected with the warm front from the west usually pushes through, bringing offshore wind. By direct wind stress, the onshore wind would produce an inward flux while an offshore wind would produce an outward flux, of water. This is generally the case as discussed earlier. The transport, however, is not obviously correlated with the northerly wind, since the correlation coefficient of the water level and the northerly wind is less than 0.30. This is probably because the frontal passage time is not exactly the time of sign change of the north component of the wind, or there is a lag between the wind and setup or setdown. Wind is a vector and is not usually in phase with the air pressure, even though they are related, but not in a linear way. This is similar to a recent study of the wind-driven transport through multiple inlets of Lake Pontchartrain (Huang and Li 2017), in which the correlation of the transport and the northerly wind component is on the order of 0.2–0.4.

In contrast, the transport and easterly wind component have generally larger correlations. In the present study, this correlation for the ''cold front season'' (late October to the following April) has an overall value of −0.59 for the first deployment and −0.39 for the second (the negative sign indicates that this is consistent with the Ekman transport—a negative or east wind would cause the coast to have a higher water level). Compared with a correlation coefficient of −0.73 to −0.78 of Huang and Li (2017), the present study shows a smaller magnitude of correlations. However, the larger magnitude of correlation between the easterly wind component and the transport than that between the northerly wind component and the transport suggests that the wind-driven Ekman transport does play an important role in the setup and setdown of the overall water level, considering the fact that the coastline in the study area along the northern Gulf of Mexico is roughly east to west. As a result, the inward and outward transports are more correlated with the east wind component as accepted in many studies, for example, Kupchik (2014).

5. Concluding remarks

A single-point bottom-mounted acoustic Doppler current profiler (ADCP) can record velocity profiles at a fixed location. It is, however, not sufficient to provide the total volume transport of water across a section. A small boat equipped with a surface-mounted ADCP can run along a planned transect to provide measurements of volume transport. The latter approach is costly and cannot be operated for long term (e.g., weeks or longer). Here, we used a combination of the two methods and established a correlation between the flow velocity from the bottom-mounted ADCP with the total transport. This study involves 1) a new technique using a combination of measurements from an ADCP on an unmanned boat (a USV) and an ADCP deployed at bottom to calculate the total transport of water in a tidal channel using a regression, and 2) results for the influence of synoptic weather on subtidal transport variations in a tidal channel.

The observational data from the bottom-mounted ADCP covered 515 days. With two surveys using the USV, one for 8 h and one for 24 h, we were able to obtain regression coefficients that had an R-squared value of ~0.98–0.99. The first EOF mode of the flow velocity profile shows a one-layer barotropic flow that explained 98.2% of the variability, while the second mode is a

typical two-layer estuarine type of flow with only 0.47% of the total variability. This means that the flow in this system is basically barotropic and stratification is very limited. For that reason, the linear regression between transport measured from the USV and depth-averaged velocity recorded from the bottom-mounted ADCP data is reliable and the regression can be extended for the entire 515 days for the transport. The second part of the study uses the 515-day time series of transport data and analyzed the impact of synoptic weather systems, particularly cold fronts and warm fronts. Using harmonic analysis, it is shown that the most regular variation is the diurnal tidal variations, with K_1 and O_1 tides dominating. It is shown that whenever there was a significant atmospheric frontal system passing the study area, whether it was a cold or warm front, there was an almost immediate response of the subtidal water transport. This immediate response is consistent with Huang and Li (2017), who show that a quasi-steady state is a surprisingly accurate approximation for low-frequency wind-driven response in cold front weather.

In the present study, there were individual cold and warm fronts, and combinations of them passing in sequence. This resulted in a complicated response of transport. Our study focuses mainly on seven of the largest such events that caused a net transport in the tidal channel at Port Fourchon of 30–40 $m^3 s^{-1}$. A correlation can be established between atmospheric parameters and the water level, velocity or transport. It is found that air pressure can be used to predict the transport most reliably (with a correlation coefficient of up to 0.82). The correlation is further confirmed with the MSC value, which showed a maximum within the ''weather band'' and the maximum occurred at ~0.2909 cpd or 3.4 days, which falls into the weather band (0.14–0.33 cpd, or 3–7 days).

It is found in this study that a cold front almost always causes a decrease in water level and an outward transport. The opposite is true for a warm front. This can be seen from all the major events discussed. The transport is basically determined by the wind of the cold front and warm front systems passing the area. Although the wind variation in these systems has some general patterns, the wind variation can be different depending on the orientation of the fronts and the direction of movement of the systems (Roberts et al. 1989; Huang and Li 2017). The conclusion is similar to that of Huang and Li (2017) for the Lake Pontchartrain estuary, but the latter work has a more in-depth discussion on remote and local wind effects, and a quasi-steady state momentum balance is found and illustrated. Unlike the work of Huang and Li (2017), the system here is a narrow tidal channel within a network of channels and therefore is not necessarily the same as the Lake Pontchartrain estuary. However, the low-frequency wind-driven flows do appear to be consistent in both studies. Our focus here is the implementation of the technique of using an unmanned boat to calibrate total transport during severe weather when a boat-based survey is not feasible or safe to implement. This method should have a broader application in the coastal region.

This work shows that in this system the linear regression to calculate the total transport from a single moored ADCP can be surprisingly accurate. This may not be guaranteed in other systems. For instance, if there is a strong lateral structure in velocity (such as that within an eddy), or a tidal phase difference, and/or strong stratification, the conclusion may be different and a linear regression is not guaranteed to be accurate. The moored ADCP flow data would have shown a similar trend in response to weather, except that we would not know the total transport and if there is any cross-channel variation that would alter the conclusion (i.e., whether the transport view and velocity view would agree with each other). From this point of view, the discussion on transport does add more information and provides a useful approach for future study in other systems. The use of an unmanned boat added a reliable technique to accurately measure the cross-channel distribution of flows. The use of a unmanned boat for measurements is easier, faster, and much more accurate in repeating planned transects, and it can be repeated many more times than using a manned boat.

Acknowledgments. The study is support by the Louisiana Board of Regents (Traditional Enhancement Project LEQSF 2016-17-ENH-TR-05), the NSF (OCE 1736713), the Northern Gulf Institute (NNS05AA95C), the Louisiana Coastal Protection and Restoration Authority (Interagency Agreement 2514-1401), NOAA/GCOOS (NOAA-NOS-IOOS-2016-2004378), BOEM (Cooperative Agreement 0104CA32806 Task Order 0106TO39901), and the National Key R/D Project of the National Science Commission of China (2017YFC1404201) through Zhejiang Ocean University (21105013015). The work was conducted by the research team of the Wave-Current-Surge Information System (WAVCIS; wavcis.csi.lsu.edu).

REFERENCES

Andrade, C. A., E. D. Barton, and C. N. K. Mooers, 2003: Evidence for an eastward flow along the Central and South American Caribbean Coast. *J. Geophys. Res.*, **108**, 3185, https://doi.org/10.1029/2002JC001549.

Barton, E. D., J. L. Largier, R. Torres, M. Sheridan, A. Trasvina, A. Souza, Y. Pazos, and A. Valle-Levinson, 2015: Coastal upwelling and downwelling forcing of circulation in a semi-enclosed bay: Ria de Vigo. *Prog. Oceanogr.*, **134**, 173–189, https://doi.org/10.1016/j.pocean.2015.01.014.

Boon, J. D., 2004: *Secretes of the Tide: Tide and Tidal Current Analysis and Predictions, Storm Surges and Sea Level Trends*. Woodhead Publishing, 224 pp.

Brown, H. C., L. K. Jenkins, G. A. Meadows, and R. A. Shuchman, 2010: *BathyBoat*: An autonomous surface vessel for standalone survey and underwater vehicle network supervision. *Mar. Technol. Soc. J.*, **44** (4), 20–29, https://doi.org/10.4031/MTSJ.44.4.5.

Buijsman, M. C., and H. Ridderinkhof, 2007a: Long-term ferry-ADCP observations of tidal currents in the Marsdiep inlet. *J. Sea Res.*, **57**, 237–256, https://doi.org/10.1016/j.seares.2006.11.004.

——, and ——, 2007b: Water transport at subtidal frequencies in the Marsdiep inlet. *J. Sea Res.*, **58**, 255–268, https://doi.org/10.1016/j.seares.2007.04.002.

Butterworth, S., 1930: On the theory of filter amplifiers. *Exp. Wireless Wireless Eng.*, **7**, 536–541.

Caccia, M., M. Bibuli, R. Bono, G. Bruzzone, G. Bruzzone, and E. Spirandelli, 2007: Unmanned surface vehicle for coastal and protected waters applications: The Charlie project. *Mar. Technol. Soc. J.*, **41** (2), 62–71, https://doi.org/10.4031/002533207787442259.

Chaigneau, A., N. Dominguez, G. Eldin, L. Vasquez, R. Flores, C. Grados, and V. Echevin, 2013: Near-coastal circulation in the Northern Humboldt Current System from shipboard ADCP data. *J. Geophys. Res. Oceans*, **118**, 5251–5266, https://doi.org/10.1002/jgrc.20328.

Codiga, D. L., 2015: A marine autonomous surface craft for long-duration, spatially explicit, multidisciplinary water column sampling in coastal and estuarine systems. *J. Atmos. Oceanic Technol.*, **32**, 627–641, https://doi.org/10.1175/JTECH-D-14-00171.1.

——, and D. A. Aurin, 2007: Residual circulation in eastern Long Island Sound: Observed transverse-vertical structure and exchange transport. *Cont. Shelf Res.*, **27**, 103–116, https://doi.org/10.1016/j.csr.2006.09.001.

Dingler, J. R., T. E. Reiss, and N. G. Plant, 1993: Erosional patterns of the Isles Dernieres, Louisiana, in relation to meteorological influences. *J. Coastal Res.*, **9**, 112–125.

Emery, W. J., and R. E. Thomson, 2004: *Data Analysis Methods in Physical Oceanography*. 2nd and rev. ed. Elsevier, 654 pp.

Feng, Z., and C. Li, 2010: Cold-front-induced flushing of the Louisiana bays. *J. Mar. Syst.*, **82**, 252–264, https://doi.org/10.1016/j.jmarsys.2010.05.015.

Firing, Y. L., T. K. Chereskin, and M. R. Mazloff, 2011: Vertical structure and transport of the Antarctic Circumpolar Current in Drake Passage from direct velocity observations. *J. Geophys. Res.*, **116**, C08015, https://doi.org/10.1029/2011JC006999.

Goudey, C., T. Consi, J. Manley, M. Graham, B. Donovan, and L. Kiley, 1998: A robotic boat for autonomous fish tracking. *Mar. Technol. Soc. J.*, **32** (1), 47–53.

Huang, W., and C. Li, 2017: Cold front driven flows through multiple inlets of Lake Pontchartrain Estuary. *J. Geophys. Res. Oceans*, **122**, 8627–8645. https://doi.org/10.1002/2017JC012977.

Joyce, T. M., 1989: On in situ ''calibration'' of shipboard ADCPS. *J. Atmos. Oceanic Technol.*, **6**, 169–172, https://doi.org/10.1175/1520-0426(1989)006<0169:OISOSA>2.0.CO;2.

Kang, K., and D. Di Iorio, 2008: A study of estuarine flow using the roving ADCP data. *Ocean Sci. J.*, **43**, 81–90, https://doi.org/10.1007/BF03020584.

Kantha, L., 2005. Barotropic tides in the Gulf of Mexico. *Circulation in the Gulf of Mexico: Observations and Models*, *Geophys. Monogr.*, Vol. 161, Amer. Geophys. Union, 159–163, https://doi.org/10.1029/161GM13.

Keen, T. R., 2002: Waves and currents during a winter cold front in the Mississippi bight, Gulf of Mexico: Implications for barrier island erosion. *J. Coastal Res.*, **18**, 622–636.

Kupchik, M. J., 2014: A study of the temporal and spatial distribution of ichthyoplankton and post-larval penaeids recruiting into a Louisiana tidal pass. Ph.D. dissertation, Louisiana State University, 353 pp.

Li, C., 2002: Axial convergence fronts in a barotropic tidal inlet—Sand Shoal Inlet, VA. *Cont. Shelf Res.*, **22**, 2633–2653, https://doi.org/10.1016/S0278-4343(02)00118-8.

——, 2006: Modeling of bathymetry-locked residual eddies in well-mixed tidal channels with arbitrary depth variations. *J. Phys. Oceanogr.*, **36**, 1974–1993, https://doi.org/10.1175/JPO2955.1.

——, 2013: Subtidal water flux through a multiple-inlet system: Observations before and during a cold front event and numerical experiments. *J. Geophys. Res. Oceans*, **118**, 1877–1892, https://doi.org/10.1002/jgrc.20149.

——, and E. Weeks, 2009: Measurements of a small scale eddy at a tidal inlet using an unmanned automated boat. *J. Mar. Syst.*, **75**, 150–162, https://doi.org/10.1016/j.jmarsys.2008.08.007.

——, and C. Chen, 2014: Shelf circulation prior to and post a cold front event measured from vessel-based acoustic Doppler current profiler. *J. Mar. Syst.*, **139**, 38–50, https://doi.org/10.1016/j.jmarsys.2014.05.006.

——, A. Valle-Levinson, L. Atkinson, and T. C. Royer, 2000: Inference of tidal elevation in shallow water using a vessel-towed ADCP. *J. Geophys. Res.*, **105**, 26 225–26 236, https://doi.org/10.1029/1999JC000191.

——, H. Roberts, G. W. Stone, E. Weeks, and Y. X. Luo, 2011a: Wind surge and saltwater intrusion in Atchafalaya Bay during onshore winds prior to cold front passage. *Hydrobiologia*, **658**, 27–39, https://doi.org/10.1007/s10750-010-0467-5.

——, J. R. White, C. Chen, H. Lin, E. Weeks, K. Galvan, and S. Bargu, 2011b: Summertime tidal flushing of Barataria Bay: Transports of water and suspended sediments. *J. Geophys. Res.*, **116**, C04009, https://doi.org/10.1029/2010JC006566.

——, X. Li, G. Zhang, K. M. Boswell, M. E. Kimball, D. Shen, and J. Lin, 2017: Estuarine plume: A case study by satellite SAR observations and in situ measurements. *IEEE Trans. Geosci. Remote Sens.*, **55**, 2276–2287, https://doi.org/10.1109/TGRS.2016.2641161.

Lin, J., C. Li, K. M. Boswell, M. Kimball, and L. Rozas, 2016: Examination of winter circulation in a northern Gulf of Mexico estuary. *Estuaries Coasts*, **39**, 879–899, https://doi.org/10.1007/s12237-015-0048-y.

Liu, Z., Y. Zhang, X. Yu, and C. Yuan, 2016: Unmanned surface vehicles: An overview of developments and challenges. *Annu. Rev. Control*, **41**, 71–93, https://doi.org/10.1016/j.arcontrol.2016.04.018.

Moeller, C. C., O. K. Huh, H. H. Roberts, L. E. Gumley, and W. P. Menzel, 1993: Response of Louisiana coastal environments to a cold front passage. *J. Coastal Res.*, **9**, 434–447.

Norcross, B. L., and R. F. Shaw, 1984: Oceanic and estuarine transport of fish eggs and larvae: A review. *Trans. Amer. Fish. Soc.*, **113**, 153–165, https://doi.org/10.1577/1548-8659(1984)113<153:OAETOF>2.0.CO;2.

Osiński, R., P. Wieczorek, A. Beszczyńska-Möller, and I. Goszczko, 2003: ADCP-referenced geostrophic velocity and transport in the West Spitsbergen Current. *Oceanologia*, **45**, 425–435.

Roberts, G. N., and R. Sutton, Eds., 2006: *Advances in Unmanned Marine Vehicles.* IET Control Engineering Series 69, Institution

of Engineering and Technology, 464 pp., https://doi.org/10.1049/PBCE069E.

——, and ——, Eds., 2012: *Further Advances in Unmanned Marine Vehicles*. IET Control Engineering Series 77, Institution of Engineering and Technology, 429 pp., https://doi.org/10.1049/PBCE077E.

Roberts, H. H., O. K. Huh, S. A. Hsu, L. J. Rouse, and D. A. Rickman, 1989: Winter storm impacts on the Chenier Plain coast of southwestern Louisiana. *Trans. Gulf Coast Assoc. Geol. Soc. Trans.*, **39**, 515–522.

Sheremet, A., U. Gravois, and V. I. Shrira, 2016: Observations of meteotsunami on the Louisiana shelf: A lone soliton with a soliton pack. *Nat. Hazards*, **84** (Suppl.), 471–492, https://doi.org/10.1007/s11069-016-2446-2.

Valle-Levinson, A., C. Li, T. Royer, and L. P. Atkinson, 1998: Flow regimes in lower Chesapeake Bay. *Cont. Shelf Res.*, **18**, 1157–1177, https://doi.org/10.1016/S0278-4343(98)00036-3.

——, K. Holderied, C. Li, and R. Chant, 2007: Subtidal flow structure at the turning region of a wide outflow plume. *J. Geophys. Res.*, **112**, C04004, https://doi.org/10.1029/2006JC003746.

Vaneck, T., J. Manley, C. Rodriguez, and M. Schmidt, 1996: Automated bathymetry using an autonomous surface craft. *Navigation*, **43**, 407–419, https://doi.org/10.1002/j.2161-4296.1996.tb01929.x.

Walker, N. D., and A. B. Hammack, 2000: Impacts of winter storms on circulation and sediment transport: Atchafalaya-Vermilion Bay region, Louisiana, U.S.A. *J. Coastal Res.*, **16**, 996–1010.

Waterhouse, A., and A. Valle-Levinson, 2010: Transverse structure of subtidal flow in a weakly stratified subtropical tidal inlet. *Cont. Shelf Res.*, **30**, 281–292, https://doi.org/10.1016/j.csr.2009.11.008.

Weeks, E., C. Li, H. Roberts, and N. Walker, 2011: A comparison of an unmanned survey vessel to manned vessels for nearshore tidal current and transport meansurements. *Mar. Technol. Soc. J.*, **45** (5), 71–77, https://doi.org/10.4031/MTSJ.45.5.7.

Welch, P. D., 1967: The use of fast Fourier transform for the estimation of power spectra: A method based on time averaging over short, modified periodograms. *IEEE Trans. Audio Electroacoust.*, **15**, 70–73, https://doi.org/10.1109/TAU.1967.1161901.

Zhu, X.-H., A. Kaneko, T. Saito, and N. Gohda, 2001: Kuroshio stream path variation and its associated velocity structures south of Shikoku, Japan. *Geophys. Res. Lett.*, **28**, 4615–4618, https://doi.org/10.1029/2001GL013730.

——, H. Nakamura, M. Dong, A. Nishina, and T. Yamashiro, 2017: Tidal currents and Kuroshio transport variations in the Tokara Strait estimated from ferryboat ADCP data. *J. Geophys. Res. Oceans*, **122**, 2120–2142, https://doi.org/10.1002/2016JC012329.